Materials Science and Engineering C 33 (2013) 2905–2913

Contents lists available at SciVerse ScienceDirect

Materials Science and Engineering C

journal homepage: www.elsevier.com/locate/msec

Biomimetic synthesis and biocompatibility evaluation of carbonated apatites template-mediated by heparin

Yi Deng [a,b], Yuhua Sun [a], Xiaofang Chen [b], Peizhi Zhu [b,c,*], Shicheng Wei [a,b,**]

[a] Department of Oral and Maxillofacial Surgery, Laboratory of Interdisciplinary Studies, School and Hospital of Stomatology, Peking University, Beijing 100081, People's Republic of China
[b] Center for Biomedical Materials and Tissue Engineering, Academy for Advanced Interdisciplinary Studies, Peking University, Beijing 100871, People's Republic of China
[c] Department of Chemistry, University of Michigan, Ann Arbor, MI 48109-1055, United States

ARTICLE INFO

Article history:
Received 22 November 2012
Received in revised form 16 February 2013
Accepted 9 March 2013
Available online 15 March 2013

Keywords:
Biomimetic synthesis
Carbonated apatite
Heparin
Biocompatibility
Template

ABSTRACT

Biomimetic synthesis of carbonated apatites with good biocompatibility is a promising strategy for the broadening application of apatites for bone tissue engineering. Most researchers were interested in collagen or gelatin-based templates for synthesis of apatite minerals. Inspired by recent findings about the important role of polysaccharides in bone biomineralization, here we reported that heparin, a mucopolysaccharide, was used to synthesize carbonated apatites *in vitro*. The results indicated that the Ca/P ratio, carbon content, crystallinity and morphology of the apatites varied depending on the heparin concentration and the initial pH value. The morphology of apatite changed from flake-shaped to needle-shaped, and the degree of crystallinity decreased with the increasing of heparin concentration. Biocompatibility of the apatites was tested by proliferation and alkaline phosphatase activity of MC3T3-E1 cells. The results suggested that carbonated apatites synthesized in the presence of heparin were more favorable to the proliferation and differentiation of MC3T3-E1 cells compared with traditional method. In summary, the heparin concentration and the initial pH value play a key role in the chemical constitution and morphology, as well as biological properties of apatites. These biocompatible nano-apatite crystals hold great potential to be applied as bioactive materials for bone tissue engineering.

1. Introduction

Biomimetic processing for inorganic material synthesis can give rise to nano-materials with improved chemical and physical properties, as well as biological properties, which is one of the recent developments in the field of biomaterials [1,2]. The biomimetic process typically involves a bottom-up approach, which begins by designing and synthesizing molecules that have the ability to self-assemble or self-organize into a higher order of a micro- or macro-scale structure. Biomineralization is a good example of the biomimetic processing of biomaterials. During biomineralization, living organisms, such as biomacromolecues, can prevent random proliferation of mineral nuclei, control the formation of minerals, and impose highly complex shapes and textures with remarkable structural hierarchy upon solid inorganic matter to produce materials that often far exceed the performance of human-made counterparts [3].

Hydroxyapatite (HA, $[Ca_{10}(PO_4)_6(OH)_2]$) is the basic component of the natural bone. In the past decade, collagens [4,5], gelatin [6,7] and peptides [8–10] have attracted extensive interest in regulating the HA nucleation and growth during the bone formation process. Wang et al. [4] demonstrated that collagen played the predominant role in the nucleation, growth, orientation and structure of bone apatite crystals. Recently, much attention has been focused on the polysaccharide in the bone, and a study showed that the organic–mineral interface in bone was predominantly polysaccharide [11]. Zhong et al. reported an acidic polysaccharide, maleic chitosan, played an important role in regulating the morphology, size and crystallinity of the inorganic minerals [12]. More recently, Li et al. [13] indicated that hyaluronic acid, one of glycosaminoglycans (GAGs) in human body, could temporarily stabilize the amorphous calcium phosphate at the early stage of mineralization. Polysaccharide with the functional segments can chelate Ca^{2+} ions and form hydrogen bonding with PO_4^{3-} and H_2O on the surface of the minerals.

Various methods have been reported to produce nanosized apatite crystals, including chemical precipitation [14], solid-state reaction [15], hydrothermal synthesis [16], sol–gel synthesis [17], emulsion technique [18] and the laser sintering approach [19], whereas, most routine approaches can't control the crystal morphology and size precisely. Therefore, much attention is paid to biomimetic synthesis because it can prepare nanosized apatite crystals with controllable size and shape by

* Correspondence to: P.Z. Zhu, Department of Chemistry, University of Michigan, Ann Arbor, MI 48109-1055, United States. Tel./fax: +1 734 7630477.
** Correspondence to: S.C. Wei, Department of Oral and Maxillofacial Surgery, Laboratory of Interdisciplinary Studies, School and Hospital of Stomatology, Peking University, No. 22 Zhong-Guan-Cun South Road, Hai-Dian District, Beijing 100081, People's Republic of China. Tel./fax: +86 10 82195780.
E-mail addresses: pzzhu@umich.edu (P. Zhu), sc-wei@pku.edu.cn (S. Wei).

0928-4931/$ – see front matter © 2013 Elsevier B.V. All rights reserved.
http://dx.doi.org/10.1016/j.msec.2013.03.016

the use of templates. Double-hydrophilic block copolymer was reported to prepare needle-like nano-hydroxyapatite crystals [20]. In addition, Li et al. successfully synthesized enamel-like HA formed on sulfonic-terminated self-assembled monolayer [21]. However, few reports employ templates containing natural glycosaminoglycans. It is necessary to understand the role of glycosaminoglycans in bone formation process.

Heparin is the most sulfated glycosaminoglycan of the extracellular matrix (ECM), which is composed of a basic unit of three sugars, N-acetyglucosamine, D-glucuronic acid and L-iduronic acid. It is a natural acidic polysaccharide with high-density negative groups, with a total of 6–7 anionic groups per tetrasaccharide consisting of 2 carboxyl and 4–5 sulfates [22]. It is mainly secreted by mast cells and basophils, and rich in liver, heart, lung and muscle [23]. Since unstable in an acid form, heparin is usually extracted and refined as a sodium salt. It is well-known that heparin is often used to treat venous thromboembolism due to high anticoagulant activity [24]. Studies have also indicated that it can relieve pain, inhibit inflammation and promote regeneration [24–26]. Heparin is currently being widely used as an injectable anticoagulant in clinical applications. Lee et al. successfully used a modified heparinized-titanium implant to enhance the osteointegration [27]. Recently, a study showed that the proper immobilization of heparin into a polypyrrole matrix by electropolymerization could promote mesenchymal stem cell differentiation towards osteoblast lineage [28]. In addition, it was reported that bone marrow-derived heparin sulfate potentiated the osteogenic activity of bone morphogenetic protein-2 (BMP-2) through increased ALP activity and osteocalcin mRNA expression [29,30]. These results show that heparin also effectively supports bone formation. However, there are no reports about apatites modified with heparin. The residual heparin on the apatites could probably relieve pain, inhibit inflammation and anticoagulation, and promote osteogenic differentiation *in vivo* bone implantation. Therefore, carbonated apatites template-mediated by heparin, are promising bone graft substitutes for bone tissue engineering in the future. A further comprehensive *in vivo* evaluation of carbonated apatites template-mediated by heparin and apatite/heparin composites is currently underway in our laboratory.

In this study, we hypothesize that negatively charged segments on heparin macromolecule played a significant role in regulating the mineralization of apatites. The purpose of the study was to investigate the effects of the concentration of heparin and the initial pH value on the chemical constitution, morphology and biocompatibility of the obtained carbonated apatites. All products were characterized by Fourier-transform infrared spectroscopy (FTIR), X-ray diffractometry (XRD), X-ray photo-electronic spectroscopy (XPS), transmission electron microscopy (TEM) and thermogravimetry analyzer (TG-DTA). The effects of obtained samples on the viability and osteogenic differentiation of MC3T3-E1 cells were measured by CCK-8 and alkaline phosphate activity assay.

2. Materials and methods

2.1. Materials

$Ca(NO_3)_2{\cdot}4H_2O$ (AR, Tianjin, China), $(NH_4)_2HPO_4$ (AR, Beijing, China), HNO_3 (AR, Beijing, China), $NH_3{\cdot}H_2O$ (AR, Tianjin, China), and heparin sodium salt (from porcine intestinal mucosa, ≥180 U/mg, Sigma Co, St. Louis, USA) were used as received without further purification.

2.2. Sample preparation

The synthesis procedure for apatites under atmospheric conditions includes heating an aqueous mixture of $Ca(NO_3)_2$ and $(NH_4)_2HPO_4$ at 95 °C for 4 h. Firstly, heparin as a template was added into $Ca(NO_3)_2$ solution before the mixed solution of $Ca(NO_3)_2$ and $(NH_4)_2HPO_4$ at the concentrations of 0, 0.15, 1, and 3 g/100 mL. Then $(NH_4)_2HPO_4$ was slowly dropped into $Ca(NO_3)_2$ solution with continuous stirring. The solutions were adjusted from the initial pH values of 2 or 7 to the final value of 10 *via* dripping nitric acid and ammonia water during the synthesis process. And the resultant white solution was aged at room temperature for 24 h. The template was not completely removed until the products were washed for at least three times with deionized water and ethanol. The as-prepared products were dried in an oven at 60 °C for 12 h before characterization. The specific synthetic condition of each sample is listed in Table 1.

2.3. Characterization

The crystalline phase of the prepared powders was examined by X-ray diffraction (XRD, Shimadzu, Tokyo, Japan) using a Cu target as radiation source ($\lambda = 1.540598$ Å) at 40 kV. The diffraction angles (2θ) were set between 20° and 60°, incremented with a step size of 4° min^{-1}. The degree of crystallinity and unit cell parameters for the carbonate-substituted apatites were also calculated using Jade 5.0 software. Fourier-transform infrared spectrometry (FTIR, Magna-IR 750, Nicolet, USA) was used to identify the functional groups of the compounds detected in the form of pellets (KBr pellet). The spectra were recorded from 4000 cm^{-1} to 400 cm^{-1}. The chemical constituent of the obtained powders was analyzed by X-ray photo-electronic spectroscopy (XPS, Kratos, UK), and the atom mol ratio of Ca to P was determined from the XPS data. Zeta potential measurements of the aqueous dispersions for the synthetic HA and the modified HA with heparin were performed using Zetasizer ZS90 (Malvern Instruments Ltd, UK). Microstructural characterization was carried out using Tecnai F20 transmission electron microscope (TEM) with an accelerating voltage of 200 kV, and selected area electron diffraction (SAED) was recorded using the same equipment. Finally thermal analysis (TG-DTA, Q600-SDT, USA) was carried out to supply the information of phase transformation of the obtained apatites, and approximately 5 mg of powders was heated from 25 °C to 1000 °C with a heating rate of 10 °C/min. All samples were carried out under a nitrogen atmosphere, with an empty Al_2O_3 crucible as a reference.

2.4. Cell culture

Mouse preosteoblast cells (MC3T3-E1, American Type Culture Collection, VA, USA) were cultured in α-Modified Eagle's Medium (Gibco, Carlsbad, CA) containing 10% fetal calf serum (Gibco), 100 μg/mL streptomycin (Amresco, Cleveland, USA) and 100 μg/mL penicillin (Amresco) at 37 °C in a humidified atmosphere of 5% CO_2.

2.5. Cell viability assay

Viability of MC3T3-E1 cells was assessed using the cell counting kit-8 assay (CCK-8, Dojindo). After cell counting, MC3T3-E1 cells were seeded in 96-well culture plates (Costar, USA) at a density of 5×10^3

Table 1
Synthesizing conditions for preparing carbonated apatites with heparin as a template.

Sample name	Heparin (g/100 mL)	$[Ca^{2+}]$ (mol/L)	$[PO_4^{3-}]$ (mol/L)	Time (h)	Temperature (°C)	pH value
Synthetic HA	0	0.167	0.1	4	95	2 → 10
pH2C0.15	0.15	0.167	0.1	4	95	2 → 10
pH2C1	1	0.167	0.1	4	95	2 → 10
pH2C3	3	0.167	0.1	4	95	2 → 10
pH7C0.15	0.15	0.167	0.1	4	95	7 → 10
pH7C1	1	0.167	0.1	4	95	7 → 10
pH7C3	3	0.167	0.1	4	95	7 → 10
pH10C0.15	0.15	0.167	0.1	4	95	10
pH10C1	1	0.167	0.1	4	95	10
pH10C3	3	0.167	0.1	4	95	10

cells/well. After seeding 24 h, cells were rinsed with phosphate buffered saline (PBS), and 200 μL medium containing different apatites with the concentration of 20 μg/mL or 200 μL pure medium (control) or 200 μL medium containing 10% dimethyl sulfoxide (DMSO) as the positive group was added to the cells. After incubating for 1, 3, and 5 days, respectively, 10 μL of CCK-8 was added into each well for 4 h incubation. Then 80 μL of supernatant from each well was transferred to new 96-well cell culture dishes. The absorbance value (OD value) was measured at 570 nm with a microplate reader (Model 680, Bio-Rad, Hercules, CA). Six specimens were tested for each incubation period, and each test was performed in triplicate.

2.6. Alkaline phosphate activity assay

Alkaline phosphatase (ALP) activity of MC3T3-E1 cells was evaluated by an assay reagent kit (Nanjing Jiancheng Bioengineering Institute, China). At the end of the incubation, cells were exposed to different nanoapatite solutions for 7 days. Cellular alkaline phosphatase activity was determined in terms of the initial rates of hydrolysis of p-nitrophenyl phosphate (Amresco) to p-nitrophenol. Briefly, the supernatant was removed and 100 μL of lysis solution (1% TritonX-100) was added into each well and incubated for 1 h. Afterwards, 30 μL of MC3T3-E1 cell lysates at each well was transferred to new 96-well cell culture dishes, and cultivated with 50 μL of carbonated buffer solution (pH = 10) and 50 μL of substrate solution (4-aminoantipyrine) at 37 °C for 15 min. Then 150 μL of potassium ferricyanide (chromogenic agent) was added into the solution above and the production of p-nitrophenol was determined by the absorbance at 520 nm in a microplate reader. For normalization, the total protein concentration was measured by a bicinchoninic acid (BCA) protein assay kit (Beijing Biosea Biotechnology, China). Thus, alkaline phosphatase activity was normalized and expressed as the total protein content (U/gprot). Six specimens were tested for each incubation period, and each test was performed in triplicate.

2.7. Statistical analysis

All quantitative data expressed as mean ± standard deviations were derived from experiments. Statistical analysis was carried out with Origin software. Student's *t*-test was used to identify the significant differences among the experimental groups, and a *p*-value of <0.05 was considered statistically significant.

3. Results and discussion

3.1. Chemical composition and morphology of apatites

3.1.1. Fourier transform infrared spectroscopy

Fig. 1 shows the FT-IR spectra of all obtained products. The typical broad peaks of the adsorbed H_2O were observed at 3444 and 1636 cm^{-1}. Both the intense peak at 3568 cm^{-1} and the weak peak at 630 cm^{-1} were associated with hydroxyl groups [31]. Existence of CO_3^{2-} originating from atmosphere observed at around 1450–1420 cm^{-1} (ν_3) and 868 cm^{-1} (ν_2), clearly showed carbonate-substituted apatites formation. It is reported that there are two types of carbonate-substituted apatites, in which PO_4^{3-} lattice site is partially substituted by CO_3^{2-} (B-type), and OH^- lattice site is substituted by CO_3^{2-} (A-type). Biological apatite is principally type B, which shows CO_3^{2-} band at about 1420 and 1455 cm^{-1}, while A-type at about 1545 and 1455 cm^{-1} [32]. So the apatites prepared by using heparin template were predominantly B-type due to the bands of CO_3^{2-} at about 1422 and 1449 cm^{-1}. The antisymmetrical stretch vibration peaks of S═O, belonged to salts $-OH-SO_2^-$, showed up at 1230 cm^{-1} [33] in the apatite sample prepared by heparin, showing the compound of HA and heparin. The intensity of peaks increased at about 1636 cm^{-1} for pH2C3, pH7C3 and pH10C3, which might result from the superimposed

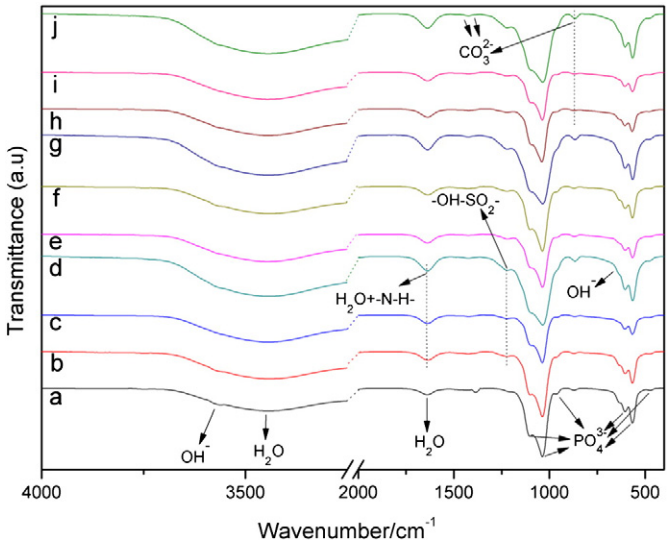

Fig. 1. FTIR spectra of obtained carbonated apatites in different conditions, and the FTIR spectrum of synthetic HA is shown for reference: (a) synthetic HA (b) pH2C0.15 (c) pH2C1 (d) pH2C3 (e) pH7C0.15 (f) pH7C1 (g) pH7C3 (h) pH10C0.15 (i) pH10C1 (j) pH10C3.

vibration of N–H and H_2O [33,34]. The bands at around 1094 and 1037 cm^{-1} were likely attributed to the triply degenerate ν_3 antisymmetric P–O stretching modes, and the peak at 962 cm^{-1} was assigned to ν_1 non-degenerate symmetric P–O bond stretching band [35]. Additionally, the peaks at about 602 and 570 cm^{-1} belonged to the triply degenerate ν_4 vibration of O–P–O bonds, and the peak at nearly 433 cm^{-1} was attributed to the ν_2 of the P–O mode [13,36]. Moreover, the characteristic peaks of heparin never occurred in curve (a) of synthetic HA.

The characteristic peaks of apatites prepared by heparin template were similar to that of synthetic HA, even though a little some differences existed. We found that at the same initial pH value (pH = 2, pH = 7 and pH = 10), the intensity of heparin peaks at around 1230 cm^{-1} and 1636 cm^{-1} increased with the increasing of heparin concentration, as well as ν_2 vibrations of CO_3^{2-} bands at 868 cm^{-1} which might be ascribed to the incremented of carbon content and more substitution of carbonate in lattice.

3.1.2. X-Ray diffraction analysis

To examine that HA was the primary calcium phosphate phase, we performed XRD analysis. The peaks on the XRD patterns of the products synthesized by heparin template (Fig. 2) at 2θ values of 25.8°, 31.7°, 32.2°, 33.0°, 46.5°, and 53.1°, indexed to (002), (211), (112), (300), (222), and (004) planes respectively, were consistent with the peaks of synthetic HA, indicating that all samples were predominantly hydroxyapatite [37]. It was obvious that the relative intensity of diffraction peaks, particularly the three most intense peaks of HA, corresponding to (211), (112), and (300) planes, decreased with the increasing of heparin concentration, implying a reduction of the crystalline degree and the dimension of apatite nano-crystals [38]. The same phenomenon was shown in apatite samples prepared under pH 7 and pH 10 conditions (Fig. 2b and Table S1). The patterns of carbonated apatites for pH2C1 and pH2C3 with lower crystallinity were very similar to those of minerals in human bone and dentin [39]. Moreover, at the same heparin concentration, the diffraction peaks of the products prepared under the neutral and the alkaline conditions were similar to those of synthetic HA. However, sharper and higher diffraction peaks were present in neutral sample, which might be ascribed to bigger sized crystals.

To further understand the structural aspect, the degree of crystallinity and unit cell parameters for carbonate-substituted apatites were also

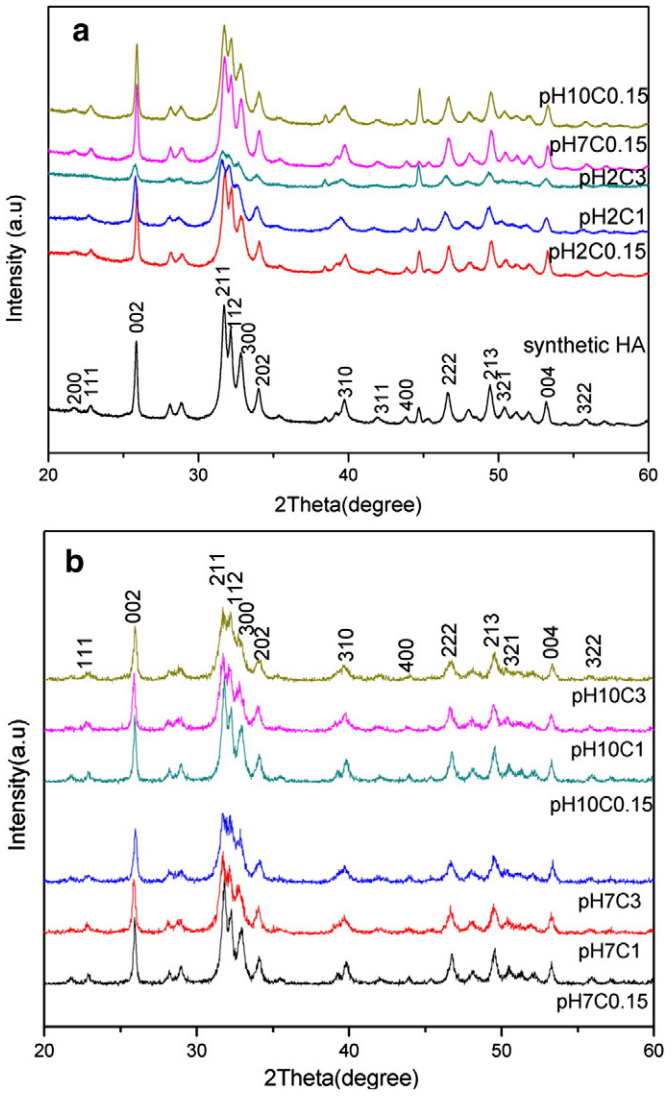

Fig. 2. (a) XRD patterns of synthetic HA, pH7C0.15, pH10C0.15 and the obtained apatites under pH2 conditions (b) the obtained apatites under pH7 and pH10 conditions. The diffraction pattern of synthetic HA is shown for reference.

calculated using Jade 5.0 software (Table 2). The lattice parameters for HA were reported to vary between 9.403 and 9.490 Å for the *a* or *b*-axis, and between 6.866 and 6.940 Å for the *c*-axis [40]. It has demonstrated that the lattice dimensions vary with the B-type carbonate content. The *a* or *b* dimension monotonically decreases, and the *c* dimension increases but not too much with the increasing carbonate content [41,42]. In addition, the degree of crystallinity also decreases as the increasing of carbon content because the deformity of crystal lattice hinders the crystallization of carbonated apatites. The dimensions of a carbonated apatites containing 4.4% CO_3^{2-} [43] and the hydroxyapatite from PDF card (JCPDS #09-0432) were used for reference. It was clear that the *c* dimension increased and the *a* dimension, as well as the degree of crystallinity, decreased, with the increasing of heparin concentration, suggesting the increasing of carbon content [41,42] which is consistent with the results of FT-IR. At the same heparin concentration, the dimensions of both neutral product and alkaline product were similar to synthetic HA. However, *a* dimension and crystallinity of pH7C0.15 were smaller than those of pH10C0.15, implying that carbonate content in pH10C0.15 was less than pH7C0.15 [41]. From above analyses and Table 2, the order of B-type carbonate content in obtained apatites was as follows: pH2C3 > HA with 4.4% CO_3^{2-} > pH2C1 > pH2C0.15 ≈ pH7C0.15 > synthetic HA ≈ pH10C0.15.

Table 2
The crystalline and lattice parameter of the as-prepared apatites in all cases. The carbonated apatites containing 4.4% CO_3^{2-} and the standard HA from PDF card (JCPDS #09-0432) are shown for reference.

Sample name	Degree of crystallinity	Lattice parameter	
		a = b(Å)	c(Å)
Synthetic HA	82.37 ± 3.2%	9.446	6.877
pH2C0.15	81.14 ± 2.6%	9.434	6.886
pH2C1	78.36 ± 3.8%	9.432	6.891
pH2C3	69.98 + 1.3%	9.411	6.894
pH7C0.15	81.29 ± 2.2%	9.440	6.878
pH10C0.15	82.80 ± 2.5%	9.447	6.876
PDF card	100%	9.418	6.884
HA with 4.3%CO_3^{2-}	/	9.425	6.892

3.1.3. X-ray photoelectron spectroscopy

X-ray photoelectron spectroscopy, an important surface analytical tool widely used in the field of biomaterials, is applied to examine the obtained apatite powders for identifying the presence of elements and for the calcium to phosphorous ratio. The XPS survey spectra and quantitative XPS analysis results are shown in Fig. 3, Fig. S1 and Table S2, indicating that calcium, phosphorus, oxygen and carbon elements were present in synthetic HA (reference sample). Other samples had the same typical characteristics as the reference sample. As discussed in FT-IR, predominantly B-type of carbonated apatites was obtained using heparin as a template. However, the Ca/P ratios of all apatites, which were very close, were all less than 1.67, showing the calcium-deficient state of apatites.

Additionally, the analysis of the elementary constituent in Table S2 shows the B-type carbonated apatites synthesized in different conditions had distinct Ca/P ratios. The carbon elements increased, but Ca/P ratio decreased with the increase of heparin concentration at the same initial pH values (pH = 2, pH = 7 and pH = 10). It illustrated that higher concentration of heparin might lead to more CO_2 absorption and lower Ca/P ratio. At the same heparin concentration and the different pH values, the products also had distinct carbon element contents, and their sequence was as follows: pH2C0.15 > pH7C0.15 > pH10C0.15,

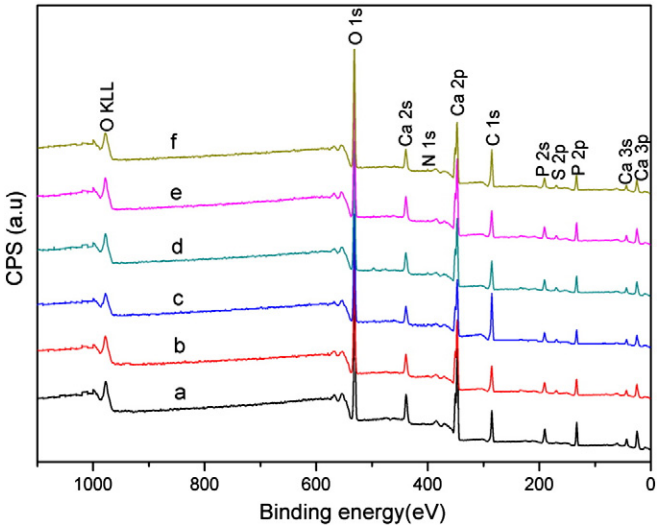

Fig. 3. XPS spectra of the obtained apatites in different conditions. The XPS survey spectrum of synthetic HA is shown for reference: (a) synthetic HA (b) pH2C0.15 (c) pH2C1 (d) pH2C3 (e) pH7C0.15 (f) pH10C0.15.

pH2C1 > pH7C1 > pH10C1 and pH2C3 > pH7C3 > pH10C3. Nitrogen and sulfur were also detected in the obtained samples using heparin as a template, and the contents of nitrogen and sulfur improved by adding heparin concentration, which verified the analysis obtained from the FTIR analysis.

3.1.4. TG-DTA studies

The representative curves of TG and DTA analysis for the obtained carbonate-substituted apatites is shown in Fig. 4. It showed that the as-prepared apatite crystals had a multistep thermolysis. The TG-DTA curves of these apatites for pH2C1 and pH2C3 were similar to that of bone [44]. Thermal decomposition residue of organic matrix absorbed on the surface of apatites can be identified by an exothermal reaction and a corresponding weight loss. The initial weight loss of all the samples around 100 °C might be ascribed to the evaporation of absorbed water with an endothermic peak (T1). The synthetic HA suffered a very slow weight loss process from room temperature to 1000 °C. On the contrary, there was a exceeding 10% weight loss between 250 °C and 500 °C for the apatites prepared by heparin with a distinct exothermic peaks (T2 ≈ 290 °C), which was attributed to the thermal degradation and pyrolyzation of the grafted heparin molecules. There were two exothermic peaks (T3 and T4) located at about 790 °C and 880 °C, corresponding to the release of carbon dioxide and OH^- ions from the decomposition of carbonated apatites, leaving oxyapatite (OAP) behind [45]. The possible reaction was described as follows:

$$Ca_{10}(PO_4)_{6-x}(OH)_2(CO_3)_y \rightarrow Ca_{10}(PO_4)_{6-x}O_{y+1} + yCO_2 + H_2O.$$

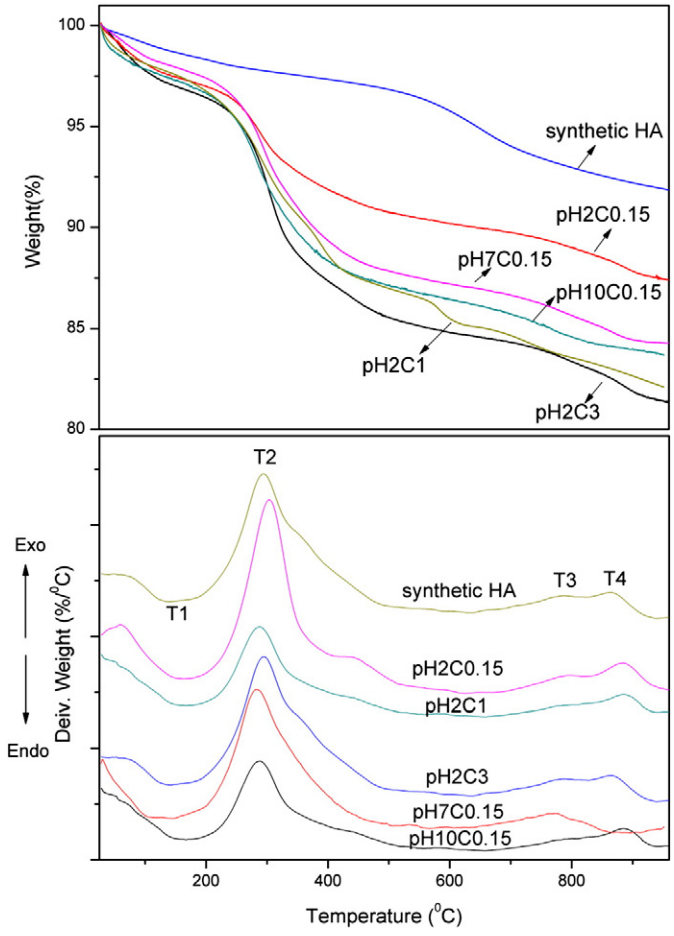

Fig. 4. TG-DTA curves for the as-prepared apatites in different conditions.

Due to the high thermal stability of HA [46], the incinerated residue of heparin–apatite compounds mainly consisted of HA. Therefore, after subtracting the water and carbon dioxide effects, the compounds of the samples can be estimated from the TG analysis, with pH2C0.15 containing about 5.6 wt.% heparin, pH2C1 containing about 10.9 wt.% heparin, pH2C3 containing about 11.5 wt.% heparin, pH7C0.15 containing about 8.1 wt.% heparin and pH10C0.15 containing about 8.3 wt.% heparin.

3.1.5. Morphology analysis by TEM

TEM image (Fig. 5) shows the morphologies of the as-prepared apatite nano-crystals using heparin as a template, from which we found that heparin concentration was an important factor for the apatites morphology. It was obviously that pH2C0.15 featured a flake-shaped morphology, and its length and diameter were not uniform, as shown in Fig. 5a. When the heparin concentration increased to 1 g/100 mL, the flake-shape of apatites became smaller, and the needle-shaped crystals appeared. Further increasing the concentration to 3 g/100 mL, only uniform needle-shaped nano-crystals with a diameter of 15–23 nm and length of 82–98 nm were obtained. It illustrated that more heparin molecular led to bigger steric hindrance, which seriously disturbed the growth of carbonate-containing apatite crystals. The initial pH value also played a significant role in the morphology and size of synthesized apatites. Both pH7C0.15 and pH10C0.15 had similar needle-shaped morphologies, which were very different from that of pH2C0.15. However, due to the alkaline hydrolysis of heparin in alkaline condition, the needles of pH10C0.15 with the size of 50–63 nm in length and 12–21 nm in width were smaller than those of pH7C0.15, as well as the size of pH10C1 compared with pH7C1 and the size of pH10C3 compared with pH7C3 (shown in Fig. 5d-i), which supported the XRD results that bigger sized crystals were present under neutral condition. Moreover, needle-shaped apatites were able to be obtained under neutral and alkaline condition when heparin concentration was at a low level (0.15 g/100 mL). The heparin macromolecules and its hydrolytic pieces as templates to attract calcium ion, promoted nucleation of apatites and guided the growth of crystals along the chains of heparin.

Moreover, the SAED patterns exhibited strong concentric rings appoint to the (002), (211) and (300) plane of apatites [47]. It also showed that the apatite precipitations had well-defined surface contours from the HRTEM image. The lattice fringes of (100) plane of apatite crystals with the lattice spacing of about 0.831 nm were showed in the HRTEM images (Fig. 5j), indicating that the longitude direction of the HA crystal was along its *c*-axis [48]. For apatite-type crystals, (100) face is more stable than (001) and (101) faces, and the crystal elongates predominantly in the <001> direction with the growth of (001) and (101) faces inhibited [49]. The fastest growth direction will form a leading tip due to the diffusion-limited growth, resulting in a needle-shaped crystal with sharp ends.

3.1.6. Energy dispersive X-ray analysis

To further verify the formation of nano-apatite particles, EDX analysis were applied to characterize their chemical composition. EDX analysis in Fig. 6 and Table S3 reveals the difference in the Ca/P ratio of the obtained apatites. These ratios differed from those calculated by XPS, but in a similar order. This was because XPS only investigates the surface elements. It was easy to find that synthetic HA and pH10C0.15 had the same Ca/P ratio closed to stoichiometric mole ratio of Ca/P = 1.67. Furthermore, at the same heparin concentration, the Ca/P ratio sequence of samples was as follows: pH7C0.15 < pH2C0.15 < pH10C0.15, implying that the alkaline condition might be good to aggregation of calcium ions on the negative groups, such as $-COO^-$ and $-SO_3^-$ groups of the templates, and led to the synthesis of apatites with high Ca/P ratio, which was the similar results reported in Li et al.'s work [13]. Moreover, It has been reported that there are interactions between Ca^{2+} of the HA and $-SO_3^-$ or $-COO-$ of heparin surface in alkaline condition [26].

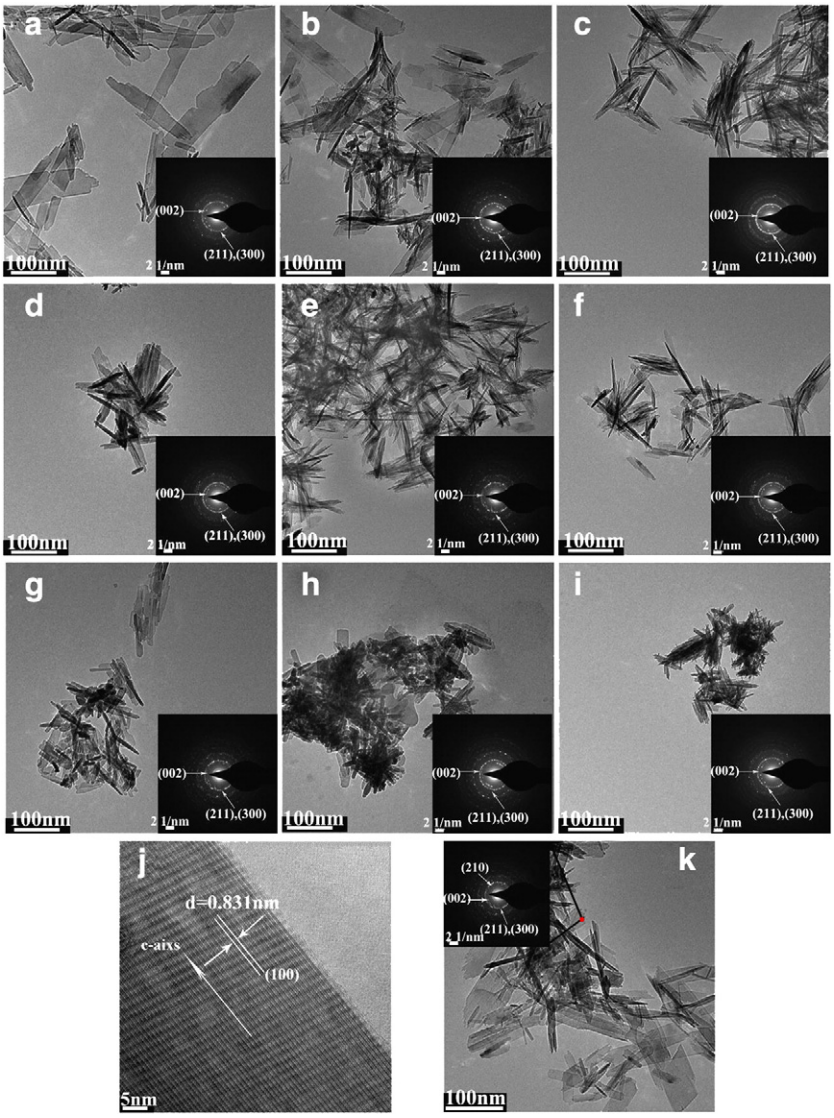

Fig. 5. TEM micrographs and SAED patterns of the carbonated apatites in different conditions: (a) pH2C0.15 (b) pH2C1 (c) pH2C3 (d) pH7C0.15 (e) pH7C1 (f) pH7C3 (g) pH10C0.15 (h) pH10C1 (i) pH10C3 (j) the HRTEM for pH2C3 (k) synthetic HA.

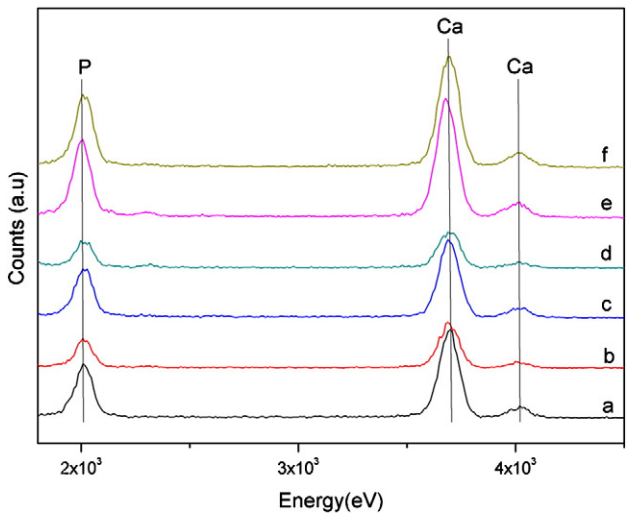

Fig. 6. TEM-associated EDX analysis of the obtained samples in different conditions. The pattern of synthetic HA is shown for reference: (a) synthetic HA (b) pH2C0.15 (c) pH2C1 (d) pH2C3 (e) pH7C0.15 (f) pH10C0.15.

3.2. The biocompatibility of carbonated apatites

3.2.1. Cell viability

The *in vitro* biocompatibility of the obtained carbonate-containing apatites was assessed by CCK-8 assay on MC3T3-E1 cell line. The viable cell number is directly proportional to the amount of CCK-8 assay products, formazan, which shows a linear response at 570 nm absorbance values. Fig. 7 shows that the OD value increased with time when MC3T3-E1 cells were co-cultured with different apatites, indicating that nanosized apatites could affected cell proliferation. It was clear that the viability of cells for 1 day displayed no statistical differences to the control group, but pH2C3 and pH10C0.15 groups showed statistical differences to pH2C0.15 group. However, after incubating for 3 and 5 days, synthetic HA, pH2C0.15, and pH2C1 groups displayed lower OD value than the control group, especially pH2C0.15 displayed the lowest absorbance. The absorbance of pH2C3 and pH7C0.15 groups were in close proximity to the control group, while pH10C0.15 group showed higher absorbance than the control group, indicating that pH10C0.15 might be able to promote the cell proliferation. The distinct OD values might be ascribed to the differences in the morphology, Ca/P ratio and carbonate content. All other apatites groups prepared by different conditions showed a large statistical difference with the pH2C0.15, and

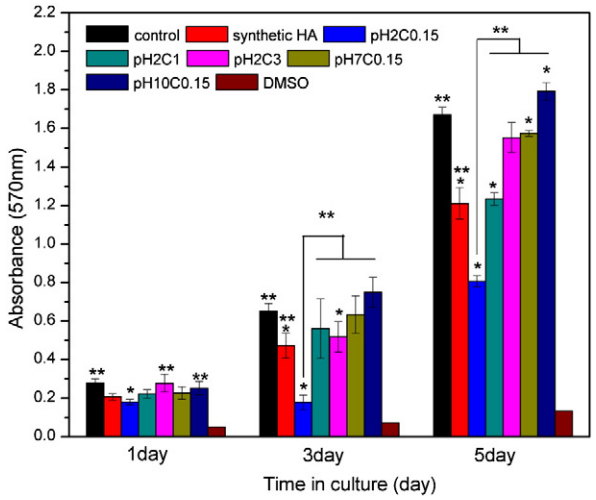

Fig. 7. Viability of MC3T3-E1 cells responding to different nano-apatites and various time points by CCK-8 analysis. * Represents $p < 0.05$ compared with the control groups, and ** represents $p < 0.05$ compared with pH2C0.15 group.

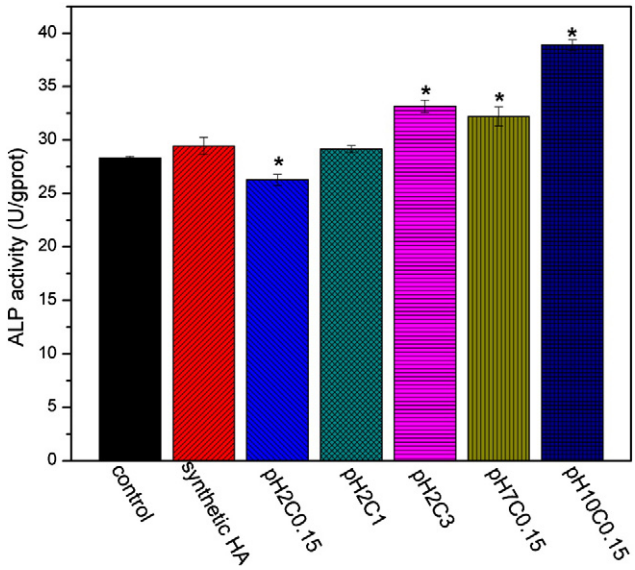

Fig. 8. ALP activity of MC3T3-E1 cell lines after culturing with the obtained apatites for 7 days. * Represents $p < 0.05$ compared with the control group.

apatites groups with needle-shaped crystals all showed the approximate or higher absorbance than the control group, suggesting that pH2C0.15 had the lowest biocompatibility mainly owing to the flake-shape. Moreover, it was reported that the crystals of biological apatite are always of a small size and that the substitution of carbonate can enhance apatites solubility, which makes HA biologically active [50]. In addition, calcium-deficient state of apatites is also of biological importance [51,52] since the catalytic activity of HA is proportional to the calcium deficiency [53]. Proper amount of carbonate, appropriate nano-morphology and non-stoichiometric Ca/P ratio may be the co-contributors to the biocompatibility of apatites.

In summary, the properties of the as-prepared carbonated apatites are listed in Table 3. From which it was observed that cells co-cultured with pH10C0.15 featured good biocompatibility. pH2C3 and pH7C0.15 also displayed very good vitality derived from its low Ca/P ratio, small size, needle-shaped morphology, as well as large amounts of carbonate substitution. However, both pH2C0.15 and pH2C1 led to very poor biocompatibility mainly due to its flake-shaped morphology. Synthetic HA featured irregular morphology which has little biological activity.

3.2.2. Alkaline phosphatase activity

Cell differentiation was investigated in terms of alkaline phosphatase activity of MC3TC-E1 cells co-cultured with apatite crystals at 7 days. Since alkaline phosphate is expressed in large amounts in the differentiation phase of MC3TC-E1 cells, the assay is able to show early osteoblastic phenotypic expressions, which is indicative of osteogenesis [54]. It can be seen from Fig. 8 that pH10C0.15, pH7C0.15, pH2C3 and pH2C0.15 groups showed differences with the control group. Furthermore, ALP activity increased along with the increasing of heparin concentration. The order of obtained apatites promoting differentiation of MC3T3-E1 was as follows: pH10C0.15 > pH2C3 > pH7C0.15 ≥ synthetic HA ≈ pH2C1 > pH2C0.15. The sequence agreed well with that of the effects of these samples on the MC3T3-E1 viability after co-culturing for 5 and 7 days, indicating that the as-prepared apatites crystals with different chemical compositions, morphology and crystallinity might have similar impacts on the growth and osteogenic differentiation of MC3T3-E1 cells.

3.3. Possible synthesis mechanism of apatites templated by heparin

Collagen, a polyanionic protein with the triple helix form, has been confirmed to play a key role in the formation of carbonated apatite in the bone. And the carboxyl-rich sequences of collagen are affirmed to be of special importance in the nucleation of apatites [4]. Heparin also has a high-density of negatively charged segments, which is similar to collagen. However, carboxyl groups and sulfate groups coexist on the chain of heparin, per tetrasaccharide consisted of 2 carboxyl and 4–5 sulfates, which is the difference of molecule structure between collagen/gelatin and heparin. It has demonstrated that the carbonated apatites templated by collagen or gelatin feature needle-shaped morphology with low degree of crystallinity [7,55,56], similar to those using heparin as the template in our work, suggesting heparin might fulfill the same functional role to control the apatite nucleation and growth as collagen and gelatin. In addition, it was reported that biomacromolecules, especially glycosaminoglycans, play a critical key role in the formation of kidney stone [57]. Recently, carboxyl or

Table 3
Properties of all obtained carbonate-containing apatite samples.

Sample name	Carbon (at.%)	Ca/P ratio	Crystallinity	OD value of cell vitality*	Morphology
Synthetic HA	27.77	1.64	82.37 ± 3.2%	Lower	Irregular
pH2C0.15	29.16	1.60	81.14 ± 2.6%	Lower	Flake-shaped
pH2C1	31.15	1.56	78.36 ± 3.8%	Lowest	Flake-shaped + needle-shaped
pH2C3	34.73	1.45	69.98 ± 1.3%	Close	Needle-shaped[a]
pH7C0.15	26.49	1.58	81.29 ± 2.2%	Close	Needle-shaped[b]
pH10C0.15	25.57	1.65	82.80 ± 2.5%	Higher	Needle-shaped[c]

[a] (89.4 ± 7.3 nm, 19.1 ± 3.6 nm).
[b] (85.7 ± 4.1 nm, 20.3 ± 5.4 nm).
[c] (56 ± 6.5 nm, 16.4 ± 3.9 nm).
* Represents comparison with the control group.

Table 4
Zeta potential characterizations of synthetic HA and the modified HA with heparin after suspending for 3 days. The tests were carried in deionized water; and the apatites received 5 minute mild sonication before test. The data expressed as mean ± standard deviations, and the sample concentrations were all 0.1 mg/ml.

Sample name	Zeta potentials in deionized water (mV)
Synthetic HA	−6.2 ± 1.1
pH2C0.15	−9.8 ± 1.4
pH2C1	−13.6 ± 0.8
pH2C3	−16.5 ± 1.0
pH7C0.15	−11.6 ± 0.5
pH10C0.15	−13.9 ± 1.3

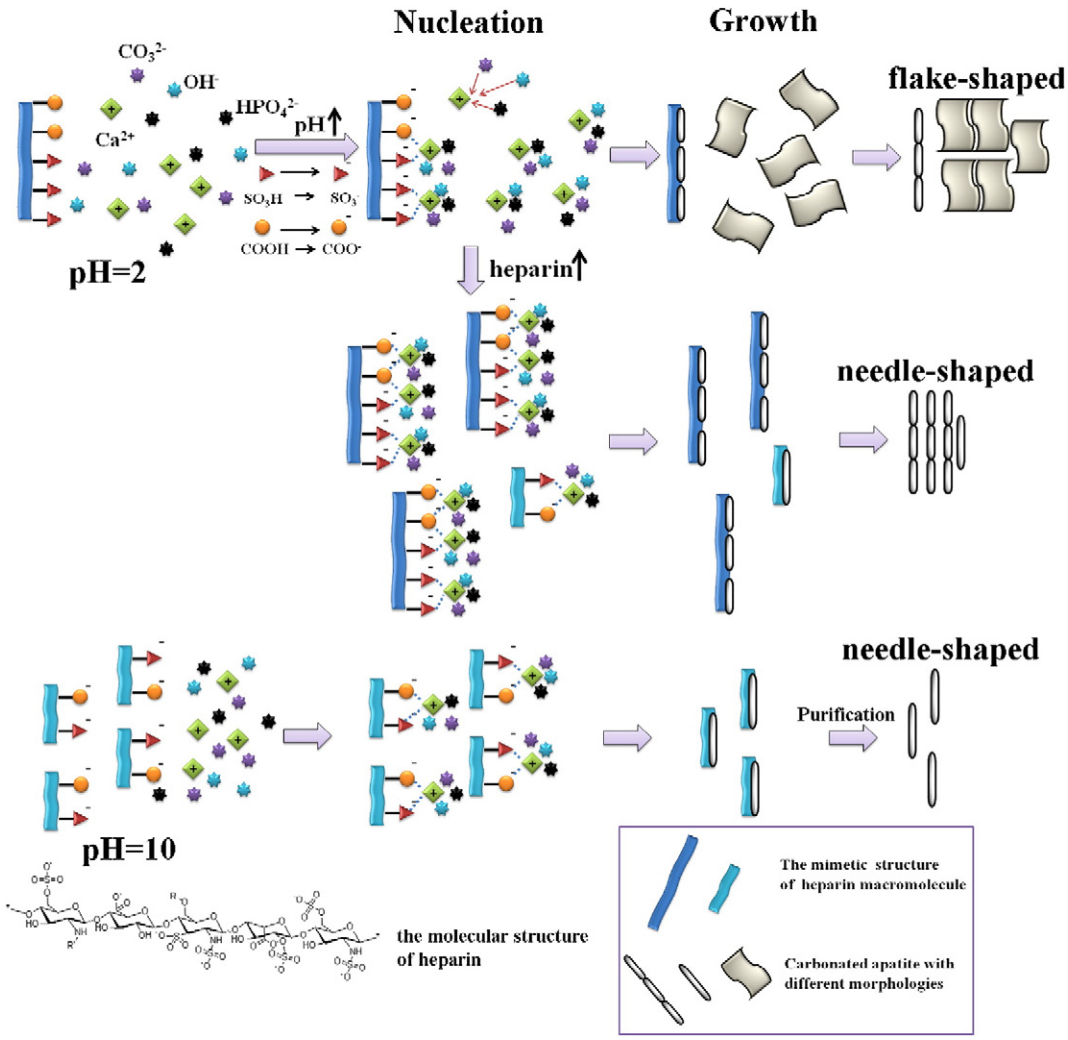

Fig. 9. Schematic drawings of carbonated apatites formation mechanism templated by heparin.

sulfate groups in GAGs contributing to the interface interaction and stabilization between mineral and organic phases in bone were demonstrated by Zhu et al. [58]. In this work, we managed to clarify how the heparin, belonging to acid GAGs, functioned as a template of apatites *in vitro*.

The zeta potentials of the synthetic HA and the modified HA with heparin were measured to validate the hypothesis. As shown in Table 4, the zeta potentials increased from -6.2 ± 1.1 to -16.5 ± 1.0 mV by adding heparin. It might be resulted from the surface decoration of the negatively charged heparin, especially, after adding hydrophilic heparin at the concentration of 3 g/100 ml, which not only confers the apatites with abundant negative charges, such as carboxyl and sulfate groups, but also influences the morphology of apatites. On the other hand, at the same heparin concentration, the zeta potentials showed distinct values for pH10C0.15, pH7C0.15 and pH2C0.15, and the values decreased from -13.9 ± 1.3 to -9.8 ± 1.4 mV when the initial pH changed from alkaline to acidic. The reason might be that the surfaces of pH10C0.15 sample were more decorated by the hydrolytic pieces of heparin, which might suggested the strong electrostatic interaction between the negative segments of heparin and Ca^{2+} of the apatites in alkaline condition. The successful decoration of heparin onto apatites was additionally confirmed by FTIR and XPS patterns. The possible mechanism is shown in Fig. 9.

At the initial pH value of 2, the $-COOH$ and $-SO_3H$ groups can't chelate calcium cations. As the solution becomes alkaline, the function groups in the form of $-COO^-$ and $-SO_3^-$ anions can chelate the Ca^{2+} and furthermore promote the nucleation of apatites. At low heparin concentration, few Ca^{2+} ions are chelated on the surface of heparin macromolecule, and nucleation of minerals mostly goes on in solution leading to flake-shaped crystals. With the increasing of heparin concentration, more Ca^{2+} ions are absorbed by the function groups of heparin, and needle-shaped inorganic crystals begin to appear on the surface of heparin chain. When heparin concentration reaches a higher level, such as 3 g/100 mL, only needles appear due to big steric hindrance of heparin macromolecules, which can chelate most Ca^{2+} ions in the solution.

When the initial pH value increased to 7, the function segments with $-COO^-$ and $-SO_3^-$ anions easily chelate Ca^{2+}, and thus form ionic nuclei for the growth of apatite crystals. Needle-shaped products grow on the surface of heparin, which functions like a natural template. Subjected to the initial pH of 10, heparin undergoes alkaline hydrolysis and goes down to pieces completely, which leads to smaller size of inorganic minerals confirmed by TEM. Thus the initial pH value and the concentration of heparin both play important roles in Ca/P ratio and carbonate content, as well as distinct morphologies, and the biological properties of apatites largely depend on its Ca/P ratio, carbonate content and morphology.

4. Conclusion

In this study, different carbonate apatite nano-crystals were prepared by biomimetic synthesis using heparin as a template for the

first time. Changing the pH value and the heparin concentration in the synthesis process can lead to the production of apatite minerals with different carbonate content, crystalline and Ca/P ratio, as well as morphology. TEM images exhibited that needle-like morphology of apatites were obtained in the presence of heparin. It is proved that the negatively charged segments on heparin macromolecule, such as the carboxyl groups and sulfate groups, could chelate Ca^{2+} ions in the solution and form ionic nuclei for the nucleation of apatites. More importantly, *in vitro* cytocompatibility tests reveal that some of carbonated apatites are favorable to the proliferation and differentiation of MC3T3-E1 cells compared to synthetic HA without heparin. Therefore, the biocompatible carbonate apatites prepared with biomimetic procedure are the promising candidates for bone tissue engineering applications.

Acknowledgment

This work was supported by State Key Development Program for Basic Research of China (Grant 2007CB936103), the Fundamental Research Funds for the Central Universities, and Peking University's 985 Grant.

Appendix A. Supplementary data

Supplementary data to this article can be found online at http://dx.doi.org/10.1016/j.msec.2013.03.016.

References

[1] H. Colfen, Nat. Mater. 9 (2010) 960–961.
[2] A. Finnemore, P. Cunha, T. Shean, S. Vignolini, S. Guldin, M. Oyen, et al., Nat. Commun. 3 (2012) 966.
[3] W. Kunz, M. Kellermeier, Science 323 (2009) 344–345.
[4] Y. Wang, T. Azaïs, M. Robin, A. Vallée, C. Catania, P. Legriel, et al., Nat. Mater. 11 (2012) 724–733.
[5] N. Roveri, G. Falini, M.C. Sidoti, A. Tampieri, E. Landi, M. Sandri, et al., Mater. Sci. Eng. C 23 (2003) 441–446.
[6] E.V. Rosseeva, J. Buder, P. Simon, U. Schwarz, O.V. Frank-Kamenetskaya, R. Kniep, Chem. Mater. 20 (2008) 6003–6013.
[7] X. Liu, L.A. Smith, J. Hu, P.X. Ma, Biomaterials 30 (2009) 2252–2258.
[8] M. Gungormus, M. Branco, H. Fong, J.P. Schneider, C. Tamerler, M. Sarikaya, Biomaterials 31 (2010) 7266–7274.
[9] J.D. Hartgerink, E. Beniash, S.I. Stupp, Science 294 (2001) 1684–1688.
[10] A. Mata, Y. Geng, K.J. Henrikson, C. Aparicio, S.R. Stock, R.L. Satcher, et al., Biomaterials 31 (2010) 6004–6012.
[11] E.R. Wise, S. Maltsev, M.E. Davies, M.J. Duer, C. Jaeger, N. Loveridge, et al., Chem. Mater. 19 (2007) 5055–5057.
[12] C. Zhong, C. Chu, J. Mater. Chem. 22 (2012) 6080–6087.
[13] Q. Li, M. Li, P. Zhu, S. Wei, J. Mater. Chem. 22 (2012) 20257–20265.
[14] E. Nejati, V. Firouzdor, M.B. Eslaminejad, F. Bagheri, Mater. Sci. Eng. C 29 (2009) 942–949.
[15] R.L. Karlinsey, A.C. Mackey, J. Mater. Sci. 44 (2008) 346–349.
[16] P. Sujaridworakun, F. Koh, T. Fujiwara, D. Pongkao, A. Ahniyaz, M. Yoshimura, Mater. Sci. Eng. C 25 (2005) 87–91.
[17] D.M. Liu, T. Troczynski, W.J. Tseng, Biomaterials 22 (2001) 1721–1730.
[18] H. Li, M. Zhu, L. Li, C. Zhou, J. Mater. Sci. 43 (2008) 384–389.
[19] F.E. Wiria, K.F. Leong, C.K. Chua, Y. Liu, Acta Biomater. 3 (2007) 1–12.
[20] X. Yao, H. Yao, G. Li, Y. Li, J. Mater. Sci. 45 (2010) 1930–1936.
[21] H. Li, W. Huang, Y. Zhang, M. Zhong, Mater. Sci. Eng. C 27 (2007) 756–761.
[22] G. Embery, G. RÖLla, J.B. Stanbury, Eur. J. Oral Sci. 87 (1979) 318–324.
[23] J. Wedemeyer, M. Tsai, S.J. Galli, Curr. Opin. Immunol. 12 (2000) 624–631.
[24] M.J.F.M. Janssen, J.K. Deegens, T.H. Kapinga, J.R. Beukhof, P.C. Huijgens, A.C. van Loenen, et al., Kidney Int. 49 (1996) 806–813.
[25] M.J. Saliba Jr., Burns 27 (2001) 349–358.
[26] D.M. Zhao, Y.X. Wang, Z.Y. Chen, R.W. Xu, G. Wu, D.S. Yu, Biomed. Mater. 3 (2008) 025016.
[27] D.W. Lee, Y.P. Yun, K. Park, S.E. Kim, Bone 50 (2012) 974–982.
[28] J. Serra Moreno, M.G. Sabbieti, D. Agas, L. Marchetti, S. Panero, J. Tissue Eng. Regen. Med., http://dx.doi.org/10.1002/term.1601.
[29] D.S. Bramono, S. Murali, B. Rai, L. Ling, W.T. Poh, Z.X. Lim, et al., Bone 50 (2012) 954–964.
[30] J. Ratanavaraporn, Y. Tabata, Acta Biomater. 8 (2012) 173–182.
[31] S.J. Kalita, S. Verma, Mater. Sci. Eng. C 30 (2010) 295–303.
[32] E. Landi, G. Celotti, G. Logroscino, A. Tampieri, J. Eur. Ceram. Soc. 23 (2003) 2931–2937.
[33] Y. Wan, C. Cao, M. Han, H. Liang, K. Ren, Y. Wang, et al., Polym. Adv. Technol. 22 (2011) 2643–2648.
[34] J. Jiang, L. Zhu, X. Li, Y. Xu, B. Zhu, J. Membr. Sci. 364 (2010) 194–202.
[35] J. Andersson, S. Areva, B. Spliethoff, M. Lindén, Biomaterials 26 (2005) 6827–6835.
[36] R. Murugan, S. Ramakrishna, J. Mater. Sci. 41 (2006) 4343–4347.
[37] S.K. Saha, A. Banerjee, S. Banerjee, S. Bose, Mater. Sci. Eng. C 29 (2009) 2294–2301.
[38] Y. Hu, X. Liu, X. Ma, A. Rawal, T. Prozorov, M. Akinc, et al., Chem. Mater. 23 (2011) 2481–2490.
[39] S. Liao, F. Watari, M. Uo, S. Ohkawa, K. Tamura, W. Wang, et al., J. Biomed. Mater. Res. B 74B (2005) 817–821.
[40] M. Boutinguiza, J. Pou, R. Comesaña, F. Lusquiños, A. de Carlos, B. León, Mater. Sci. Eng. C 32 (2012) 478–486.
[41] M. Vignoles, G. Bonel, D. Holcomb, R. Young, Calcif. Tissue Int. 43 (1988) 33–40.
[42] Y. Lee, Y. Hahm, S. Matsuya, M. Nakagawa, K. Ishikawa, J. Mater. Sci. 42 (2007) 7843–7849.
[43] J. Elliott, R. Wilson, S. Dowker, Adv. X-Ray Anal. 45 (2002) 172–181.
[44] Z. Yang, Y. Jiang, L. Yu, B. Wen, F. Li, S. Sun, et al., J. Mater. Chem. 15 (2005) 1807.
[45] C.J. Liao, F.H. Lin, K.S. Chen, J.S. Sun, Biomaterials 20 (1999) 1807–1813.
[46] T.I. Ivanova, O.V. Frank-Kamenetskaya, A.B. Kol'tsov, V.L. Ugolkov, J. Solid State Chem. 160 (2001) 340–349.
[47] J. Xiao, Y. Zhu, Q. Ruan, Y. Liu, Y. Zeng, F. Xu, et al., Cryst. Growth Des. 10 (2010) 1492–1499.
[48] H. Chen, B.H. Clarkson, K. Sun, J.F. Mansfield, J. Colloid Interface Sci. 288 (2005) 97–103.
[49] T. Suzuki, I. Kumeda, K. Teshima, S. Oishi, Chem. Phys. Lett. 421 (2006) 343–347.
[50] F. Driessens, Ann. N. Y. Acad. Sci. 523 (1988) 131–136.
[51] S.V. Dorozhkin, J. Mater. Sci. 42 (2007) 1061–1095.
[52] T. Narasaraju, D. Phebe, J. Mater. Sci. 31 (1996) 1–21.
[53] J.A.S. Bett, L.G. Christner, W.K. Hall, J. Am. Chem. Soc. 89 (1967) 5535–5541.
[54] S. Hattar, A. Berdal, A. Asselin, S. Loty, D. Greenspan, J. Sautier, Eur. Cell Mater. 4 (2002) 61–69.
[55] N. Nassif, F. Gobeaux, J. Seto, E. Belamie, P. Davidson, P. Panine, et al., Chem. Mater. 22 (2010) 3307–3309.
[56] F. Nudelman, K. Pieterse, A. George, P.H.H. Bomans, H. Friedrich, L.J. Brylka, et al., Nat. Mater. 9 (2010) 1004–1009.
[57] D.G. Reid, G.J. Jackson, M.J. Duer, A.L. Rodgers, J. Urol. 185 (2011) 725–730.
[58] P. Zhu, J. Xu, N. Sahar, M.D. Morris, D.H. Kohn, A. Ramamoorthy, J. Am. Chem. Soc. 131 (2009) 17064–17065.